Serine-Threonine Kinases Encoded by Split *hipA* Homologs Inhibit Tryptophanyl-tRNA Synthetase

Stine Vang Nielsen,[a] Kathryn Jane Turnbull,[a]* Mohammad Roghanian,[a]* Rene Bærentsen,[b] Maja Semanjski,[c] Ditlev E. Brodersen,[b] Boris Macek,[c] Kenn Gerdes[a]

[a]Centre for Bacterial Stress Response and Persistence, Section for Functional Genomics, Department of Biology, University of Copenhagen, Copenhagen, Denmark
[b]Centre for Bacterial Stress Response and Persistence, Department of Molecular Biology and Genetics, Aarhus University, Aarhus, Denmark
[c]Proteome Center Tübingen, Interfaculty Institute for Cell Biology, University of Tübingen, Tübingen, Germany

ABSTRACT Type II toxin-antitoxin (TA) modules encode a stable toxin that inhibits cell growth and an unstable protein antitoxin that neutralizes the toxin by direct protein-protein contact. *hipBA* of *Escherichia coli* strain K-12 codes for HipA, a serine-threonine kinase that phosphorylates and inhibits glutamyl-tRNA synthetase. Induction of *hipA* inhibits charging of glutamyl-tRNA that, in turn, inhibits translation and induces RelA-dependent (p)ppGpp synthesis and multidrug tolerance. Here, we describe the discovery of a three-component TA gene family that encodes toxin HipT, which exhibits sequence similarity with the C-terminal part of HipA. A genetic screening revealed that *trpS* in high copy numbers suppresses HipT-mediated growth inhibition. We show that HipT of *E. coli* O127 is a kinase that phosphorylates tryptophanyl-tRNA synthetase *in vitro* at a conserved serine residue. Consistently, induction of *hipT* inhibits cell growth and stimulates production of (p)ppGpp. The gene immediately upstream from *hipT*, called *hipS*, encodes a small protein that exhibits sequence similarity with the N terminus of HipA. HipT kinase was neutralized by cognate HipS *in vivo*, whereas the third component, HipB, encoded by the first gene of the operon, did not counteract HipT kinase activity. However, HipB augmented the ability of HipS to neutralize HipT. Analysis of two additional *hipBST*-homologous modules showed that, indeed, HipS functions as an antitoxin in these cases also. Thus, *hipBST* constitutes a novel family of tricomponent TA modules where *hipA* has been split into two genes, *hipS* and *hipT*, that function as a novel type of TA pair.

IMPORTANCE Bacterial toxin-antitoxin (TA) modules confer multidrug tolerance (persistence) that may contribute to the recalcitrance of chronic and recurrent infections. The first high-persister gene identified was *hipA* of *Escherichia coli* strain K-12, which encodes a kinase that inhibits glutamyl-tRNA synthetase. The *hipA* gene encodes the toxin of the *hipBA* TA module, while *hipB* encodes an antitoxin that counteracts HipA. Here, we describe a novel, widespread TA gene family, *hipBST*, that encodes HipT, which exhibits sequence similarity with the C terminus of HipA. HipT is a kinase that phosphorylates tryptophanyl-tRNA synthetase and thereby inhibits translation and induces the stringent response. Thus, this new TA gene family may contribute to the survival and spread of bacterial pathogens.

KEYWORDS persistence, ppGpp, toxin/antitoxin systems, translation, tRNA synthetase

P rokaryotic toxin-antitoxin (TA) modules are usually composed of two elements, a toxin that can inhibit cell growth and an antitoxin that counteracts the inhibitory effect of the toxin (1, 2). Based on the molecular modes of antitoxin activity, TA modules have been divided into different types (3). The abundant type II modules are charac-

terized by protein antitoxins that bind directly to and inhibit their cognate toxins by tight molecular interaction. Type II antitoxins usually contain a DNA-binding motif used to regulate TA operon transcription via binding to operators in the promoter region and a separate domain that interacts with and neutralizes the cognate toxin. Moreover, antitoxins are degraded by cellular proteases, such as Lon and/or Clp, and the cellular activity and amount synthesized of a given toxin are thus determined by the concentration of cognate antitoxin (4).

Type II modules are highly abundant; that is, most prokaryotic chromosomes encode at least one and some chromosomes encode cohorts of them. For example, *Mycobacterium tuberculosis* has 88 known, well-conserved type II TAs, while the insect pathogen *Photorhabdus luminescens* has a similarly large cohort (5). Toxin gene similarities were used to divide type II modules into superfamilies (6, 7). Thus, in general, toxins that exhibit sequence similarity inhibit cell growth by identical or related molecular mechanisms and can be grouped into the same family. Type II toxins belonging to the RelE, MazF, VapC, HipA, and TacT families curtail cell growth by inhibiting translation, CcdB and ParE inhibit DNA replication, Zeta toxins inhibit cell wall synthesis, and RES toxins inhibit cell growth by depleting NAD^+ (8–18).

The biological functions of TAs have been debated. For type II modules, many studies now point to a function in survival during stress, including tolerance of multiple antibiotics (1). Stochastic or stress-induced activation of TA modules can protect bacteria from unfavorable environmental conditions by inducing persister formation (19, 20), a transient, slow-growing state in which the bacteria are tolerant of antibiotics and various other forms of stress (21). The stochastic formation of persisters is due to phenotypic heterogeneity in clonal populations of cells and can be viewed as a bet-hedging strategy that increases the survival rate in rapidly changing environments (22). Moreover, sublethal concentrations of antibiotics and other stresses have been found to stimulate the formation of persisters (23, 24).

The first gene associated with persistence was *hipA* (high persister gene A) of *Escherichia coli* strain K-12, identified as a gain-of-function allele, *hipA7* (25). This allele, found also in clinical isolates of uropathogenic *E. coli* (26), showed a 100- to 1,000-fold increase in persistence due to two amino acid changes in HipA (changes of G to S at position 22 [G22S] and D to A at positions 291 [D291A]) (27). The *hipA* toxin gene and the upstream *hipB* antitoxin gene together constitute a type II TA module (28). Modest ectopic expression of wild-type HipA causes severe growth inhibition that can be countered by the HipB antitoxin, which interacts directly with HipA (28). HipA and HipB form a complex that represses *hipBA* transcription via binding to operators in the promoter region (26). HipA is a Hanks serine-threonine kinase (29, 30) and was found to specifically phosphorylate and inhibit glutamyl-tRNA synthetase (GltX or GltRS), causing strong inhibition of translation and induction of guanosine tetra- and pentaphosphate [(p)ppGpp] synthesis and persistence (11, 31, 32). HipA-mediated phosphorylation of the conserved residue Ser239 inhibits the activity of GltX (11), thereby preventing charging of $tRNA^{Glu}$. As a consequence, the ratio of charged to uncharged $tRNA^{Glu}$ decreases, which in turn stimulates binding of RelA-tRNA complexes to the ribosome, leading to activation of RelA (33). The resulting increase in the cellular (p)ppGpp level triggers the stringent response (11, 27, 32).

Here, we describe a novel family of three-component TA modules encoding toxins exhibiting sequence similarity to HipA. We discovered that HipT of the enteropathogenic *E. coli* O127:H6 strain E2348/69 ($HipT_{O127}$) is a toxin that can be counteracted by overproduction of tryptophanyl-tRNA synthetase (TrpS or TrpRS). Consistently, our *in vitro* data show that $HipT_{O127}$ is a serine-threonine kinase that inhibits translation by phosphorylating TrpS. $HipT_{O127}$ aligns colinearly with HipA but lacks ~100 amino acids (aa) at its N terminus (Fig. 1A). Interestingly, $hipT_{O127}$ is preceded by $hipS_{O127}$, encoding $HipS_{O127}$ (103 aa), which exhibits sequence similarity with the N-terminal part of HipA that is missing from $HipT_{O127}$ (Fig. 1A). Finally, $hipS_{O127}$ is preceded by a gene encoding a HipB homolog containing a helix-turn-helix (HTH) DNA-binding motif. HipB, HipS, and HipT form a complex *in vivo* and *in vitro*, and $HipS_{O127}$ alone counteracts $HipT_{O127}$
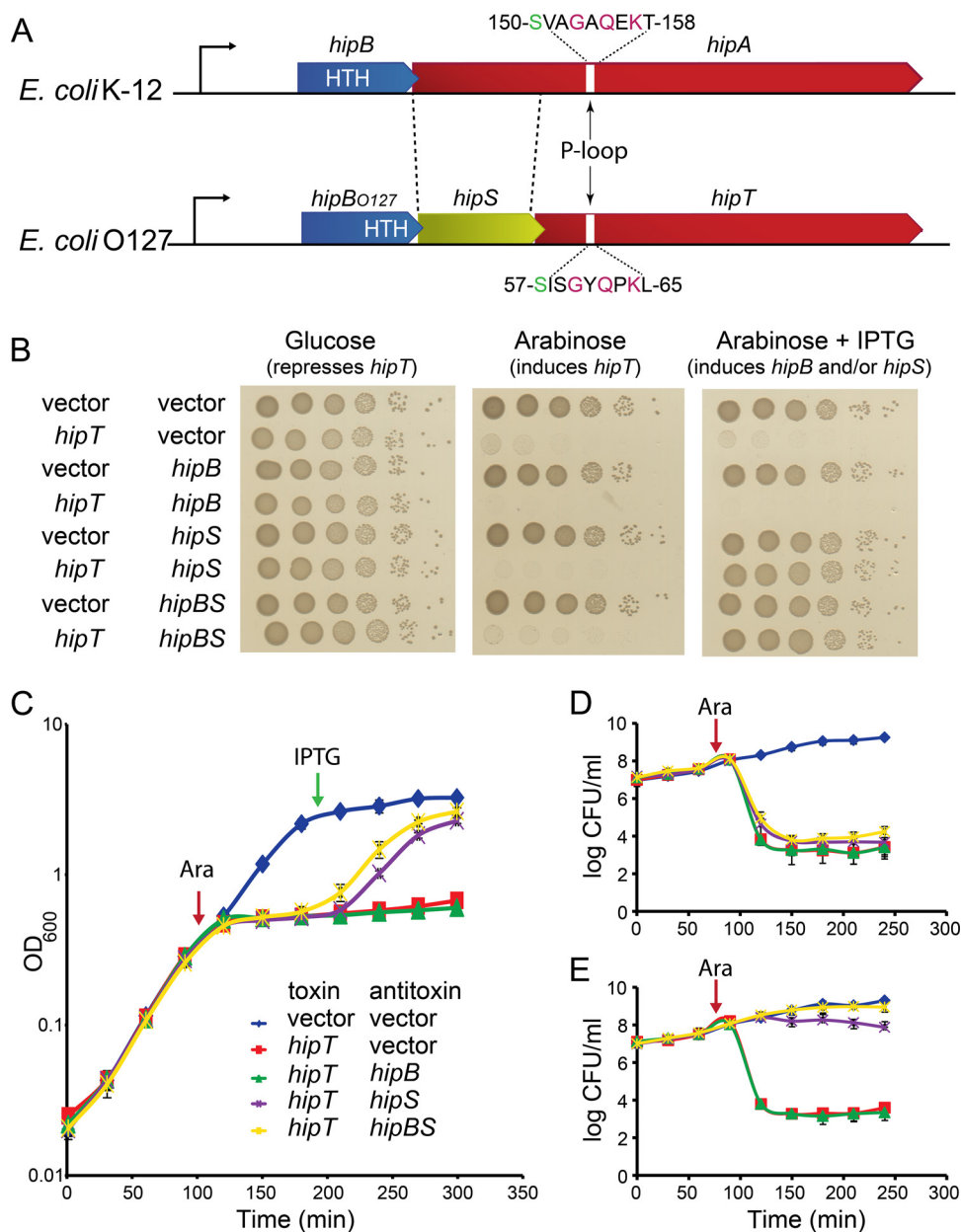
FIG 1 *hipBST* of *E. coli* O127 encodes a three-component toxin-antitoxin module. (A) Schematic showing a comparison of the *hipBA* and *hipBST* operons of *E. coli* K-12 and O127, respectively. Bent arrows pointing right indicate promoters. The *hipBA* operon contains two genes, *hipB* and *hipA*, while *hipBST*$_{O127}$ contains three genes, *hipB*$_{O127}$, *hipS*$_{O127}$, and *hipT*$_{O127}$. The region of *hipA* between the dashed lines exhibits sequence similarity to *hipS*$_{O127}$. The 8 amino acid residues of the P loop in HipA (150-VAGAQEKT-158) that binds phosphates of ATP are shown; the autophosphorylated S150 residue is shown in green (35). The homologous P loop and autophosphorylated serine in HipT$_{O127}$ were inferred by sequence similarity. (B) Overnight cultures of *E. coli* MG1655 harboring pSVN1 (pBAD33::*hipT*$_{O127}$) or the empty pBAD33 vector combined with pSVN111 (pNDM220::*hipB*$_{O127}$), pSVN109 (pNDM220::*hipS*$_{O127}$), pSVN110 (pNDM220::*hipBS*$_{O127}$), or the empty low-copy-number pNDM220 vector, as indicated, were diluted to obtain the same values of OD$_{600}$, centrifuged at 5,000 rpm for 5 min, washed in phosphate-buffered saline (PBS), and serially diluted before being spotted onto LB nutrient agar plates containing 0.2% glucose (to repress *hipT*$_{O127}$), 0.2% arabinose (to induce *hipT*$_{O127}$), or 0.2% arabinose plus 200 μM IPTG (to induce *hipB*$_{O127}$, *hipS*$_{O127}$, or *hipBS*$_{O127}$). (C) The strains used in the experiment whose results are shown in panel B were grown in LB medium plus appropriate antibiotics. Overnight cultures were diluted, cells were grown exponentially for at least 3 h until the doubling time appeared constant, and at an OD$_{600}$ of ≈0.3, arabinose (0.2%) was added to induce *hipT*$_{O127}$ (red arrow). After a further 1.5 h, IPTG (200 μM) was added to induce *hipS*$_{O127}$, *hipB*$_{O127}$, or *hipBS*$_{O127}$ (green arrow). (D and E) Viable counts of strains from the experiment whose results are shown in panels B and C before and after the addition of arabinose (0.2%) at an OD$_{600}$ of ≈0.3 (red arrow). At each time point, cell samples (0.5 ml) were washed in PBS before a 10-times dilution series was spotted on agar plates with glucose (0.2%) to repress *hipT*$_{O127}$ expression (D) or with glucose (0.2%) to repress *hipT*$_{O127}$ expression and IPTG (200 μM) to induce *hipB*$_{O127}$, *hipS*$_{O127}$, or *hipBS*$_{O127}$ (E). Plates were incubated for 16 h at 37°C before counting. Data points in panels C, D, and E represent mean values of results from at least three independent experiments, and error bars indicate standard deviations.

activity *in vivo*. The HipB homolog (called HipB$_{O127}$) does not counteract HipT$_{O127}$ but instead augments the ability of HipS$_{O127}$ to counteract HipT$_{O127}$. Analysis of the *hipBST* modules of *Haemophilus influenzae* and *Tolumonas auensis* revealed that the HipT proteins of these organisms also are counteracted by overproduction of TrpS. Moreover, cognate HipS neutralizes HipT in both these cases. In summary, we describe here a family of novel three-component TA modules that potentially can increase the stress resilience and spread of bacterial pathogens.

RESULTS

Homologs of HipA are encoded by three-gene operons. Using similarity searching with HipA (440 amino acids [aa]) of *E. coli* K-12 as the query sequence, we identified a number of genes encoding HipA homologs that aligned colinearly with the C terminus of HipA but were shortened by ~100 aa at their N termini (Fig. 1A, and see Fig. S1A in the supplemental material) (34). The HipA homologs contain P-loop motifs matching the experimentally validated P loop of HipA, as well as conserved catalytic domains and Mg^{2+} binding motifs, suggesting that, like HipA, HipT proteins are kinases (Fig. S1A) (35). A phylogenetic analysis showed that HipA and HipT group monophyletically in a cladogram based on 8 HipA and 40 HipT sequences (Fig. S1D) (36). The majority of the *hipT* genes were from gammaproteobacteria, but two HipT homologs deeply embedded in the phylogenetic tree were from a *deltaproteobacterium* and a firmicute (*Streptococcus pneumoniae*) (Fig. S1D). The HipT homolog from *S. pneumoniae* is identical to the HipT homolog of *H. influenzae* strain 10810 (Fig. S1D). These two organisms separated more than a billion years ago, and both are highly competent for DNA uptake and live in the same biological habitat (the upper respiratory tract). These observations raise the possibility that *hipBST* loci undergo lateral gene transfer between distantly related organisms.

In all the *hipT*-containing organisms examined, we discovered short open reading frames adjacent to and upstream from *hipT*, which are herein called *hipS*, encoding proteins of ~100 aa that exhibit sequence similarity to the missing N-terminal part of HipA (Fig. S1B). In all these cases, open reading frames upstream from *hipS* encode putative proteins of ~100 aa containing HTH DNA-binding motifs (Fig. S1C). These putative HipB homologs may thus autoregulate the *hipBST* operons. We chose the *hipBST* module of *E. coli* O127:H6 strain E2348/69 as our primary model system for functional analysis (Fig. 1A). The *hipBST$_{O127}$* module encodes HipB$_{O127}$ (107 aa), HipS$_{O127}$ (103 aa), and HipT$_{O127}$ (335 aa). Gene pair *hipB$_{O127}$* and *hipS$_{O127}$* overlaps by 16 nucleotides (nt), and gene pair *hipS$_{O127}$* and *hipT$_{O127}$* overlaps by 1 nt, suggesting that the genes may be translationally coupled.

HipT$_{O127}$ inhibits cell growth and is counteracted by HipS$_{O127}$. We validated the components encoded by *hipBST$_{O127}$* experimentally by inserting *hipT$_{O127}$* into plasmid vector pBAD33 (carrying the arabinose-inducible pBAD promoter) and *hipS$_{O127}$*, *hipB$_{O127}$*, and *hipBS$_{O127}$* into the low-copy-number R1 vector pNDM220 (carrying the synthetic, isopropyl-β-D-thiogalactopyranoside [IPTG]-inducible pA1/O4/O3 promoter) and subjected the standard *E. coli* K-12 strain MG1655 carrying combinations of these plasmids to growth assays and viable-count measurements. Induction of *hipT$_{O127}$* resulted in strong inhibition of cell growth, both on plates and in liquid medium, supporting the hypothesis that HipT$_{O127}$ can function as a toxin (Fig. 1B and C). Growth was rescued by induction of *hipS$_{O127}$* alone but not by *hipB$_{O127}$* alone, suggesting that HipS$_{O127}$ functions as the antitoxin (Fig. 1B and C). Coinduction of *hipB$_{O127}$* and *hipS$_{O127}$* provided a consistent, yet mild growth rescue advantage compared to the results for *hipS$_{O127}$* alone, suggesting that HipB$_{O127}$ augments the antitoxin activity of HipS$_{O127}$ (Fig. 1C). Thus, HipB$_{O127}$ does not function as a classical antitoxin.

Upon induction of *hipT$_{O127}$*, CFU decreased dramatically (Fig. 1D). However, later induction of *hipS$_{O127}$* or *hipS$_{O127}$* plus *hipB$_{O127}$* (by adding IPTG and glucose to the agar plates to induce P$_{A1/O4/O3}$::*hipBS$_{O127}$* and repress pBAD::*hipT$_{O127}$*, respectively) fully rescued cell viability (Fig. 1E). This result showed that ectopic production of HipT$_{O127}$ induces a bacteriostatic condition from which the cells can be resuscitated. In support

of this conclusion, strains in which $hipT_{O127}$ was induced recovered viability after prolonged incubation times (~40 h), even in the absence of $hipS_{O127}$ or $hipBS_{O127}$ (Fig. S2).

We were puzzled by the observation that $HipS_{O127}$ but not $HipB_{O127}$ exhibited antitoxin activity and therefore decided to analyze the $hipBST$ modules of two additional gammaproteobacteria, *Haemophilus influenzae* Rd KW20 ($hipBST_{Hi}$) and *Tolumonas auensis* DSM 9187 ($hipBST_{Ta}$) (Fig. S1). Induction of $hipT_{Hi}$ or $hipT_{Ta}$ inhibited cell growth of *E. coli* MG1655 in liquid medium in both cases, and induction of cognate $hipS$ genes was sufficient to neutralize the two HipT toxins (Fig. S3A and B). Like $HipB_{O127}$, $HipB_{Hi}$ augmented the ability of $HipS_{Hi}$ to neutralize $HipT_{Hi}$, as the presence of the $HipBS_{Hi}$-encoding plasmid almost entirely prevented growth inhibition after induction of $hipT_{Hi}$ (Fig. S3A). $HipB_{Ta}$ did not detectably augment the antitoxin effect of $HipS_{Ta}$ in this experimental setup (Fig. S3B). We also tested $hipT$ genes from strains of *Vibrio cholerae* and *Vibrio halioticoli*, but their induction was, for unknown reasons, not toxic in *E. coli* K-12 and the corresponding $hipBST$ modules were not analyzed further.

HipB, HipS, and HipT form a ternary complex *in vivo*. The above-described observations suggest that $HipB_{O127}$, $HipS_{O127}$, and $HipT_{O127}$ might form a protein complex *in vivo*, as seen for other type II TA modules. To test this, we constructed a plasmid (pSVN94) encoding N-terminally His_6-tobacco etch virus (TEV)-tagged $HipB_{O127}$, $HipS_{O127}$, and the enzymatically inactive $HipT_{O127}^{D233Q}$ mutant protein in which all three genes had optimized translation signals (Shine-Dalgarno [SD] sequences and ATG start codons) to increase translation rates. His_6-TEV-$HipB_{O127}$ was purified under native conditions and analyzed by denaturing polyacrylamide gel electrophoresis (SDS-PAGE). Indeed, three proteins of the expected molecular weights (MWs) copurified (Fig. S4A), indicating that the $HipBST_{O127}$ proteins form a complex *in vivo*. Further separation of the protein complex using a heparin column allowed isolation of three samples containing $HipT_{O127}$, $HipBT_{O127}$, and $HipBST_{O127}$ (Fig. S4B, top). Gel filtration chromatography further confirmed that HipT and HipBST are monodispersed in solution, suggesting that $HipBST_{O127}$ is a heterotrimer (Fig. S4B, bottom).

Multicopy suppression of HipT by *trpS*. Previously, we showed that overproduction of GltX suppresses HipA-mediated growth inhibition and that HipA phosphorylates GltX *in vitro* (11). Unexpectedly, overproduction of GltX did not suppress HipT-mediated growth inhibition (Fig. S5A). Therefore, we performed a second multicopy gene library screening in an attempt to identify genes that in high copy numbers could suppress the effect of $HipT_{O127}$ (see Materials and Methods). Using a pBR322-based Sau3A-derived gene library of *E. coli* MG1655Δ*ydeA*, ~8,300 colonies with an average insert size of ~3,300 bp were screened, resulting in a coverage of roughly 5.8 times. In this screening, 105 hits were obtained, of which 19 were retransformed. Six of these plasmids exhibited a stable phenotype and were sent for sequencing. Thereby, we identified a DNA fragment containing *rpe*, *gph*, and *trpS* that suppressed $HipT_{O127}$. Of these genes, only conditional induction of *trpS*, which encodes tryptophanyl-tRNA synthetase (TrpS), suppressed $HipT_{O127}$-mediated growth inhibition, both on solid medium (Fig. S5B) and in liquid culture (Fig. 2A). TrpS also suppressed $HipT_{Hi}$ and $HipT_{Ta}$ (Fig. 2B and C and Fig. S5B), whereas GltX had no such effect (Fig. S5A).

HipT phosphorylates TrpS at a conserved sequence motif. The above-described results suggested that HipT phosphorylates TrpS. To analyze HipT kinase activity directly, we purified $HipT_{O127}$ and its presumed target, TrpS. For comparison, we included HipA and its known target GltX in the analysis. Indeed, $HipT_{O127}$ phosphorylated TrpS *in vitro* (Fig. 3A, lanes 5 and 8) in a reaction that did not require tRNA (Fig. S6). We showed previously that HipA phosphorylates GltX *in vitro* in a reaction that requires the addition of tRNA^{Glu} (11). Here, we were able to reproduce the results showing that HipA phosphorylates GltX in the presence but not in the absence of tRNA (Fig. 3B, lanes 6 and 9). Thus, HipT and HipA kinases differ not only with respect to their specific target but also by whether there is a requirement for the presence of tRNA in the *in vitro* reaction mixtures (see Discussion).
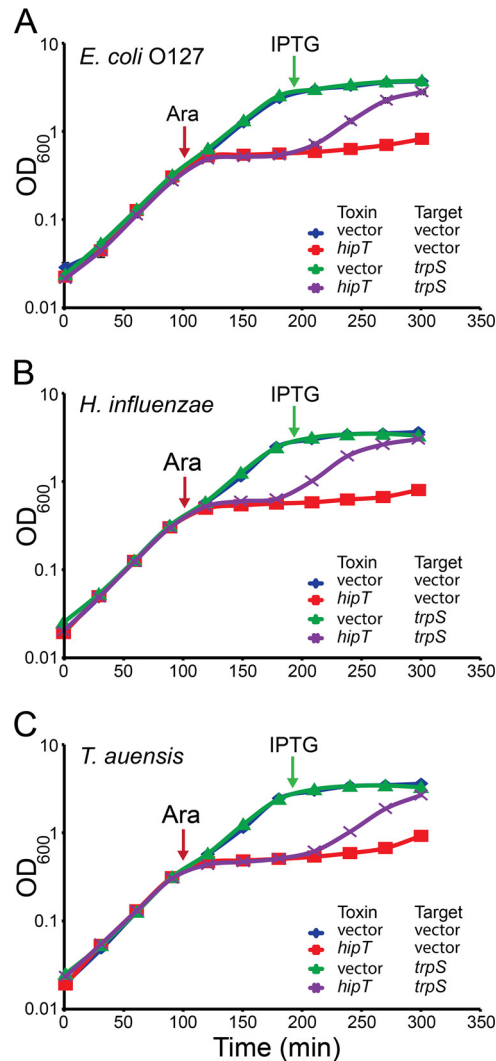
FIG 2 Overproduction of TrpS counteracts HipT$_{O127}$. (A to C) Growth curves of strains of *E. coli* MG1655 harboring pSVN1 (pBAD33::*hipT$_{O127}$*) (A), pSVN135 (pBAD33::*hipT$_{Hi}$*) (B), and pSVN129 (pBAD33::*hipT$_{Ta}$*) (C) or the empty pBAD33 vector combined with pSVN37 (pEG25::*trpS*) or the empty high-copy-number pEG25 vector, as indicated. Cells were grown in LB medium supplemented with the appropriate antibiotics. Overnight cultures were diluted and grown exponentially for at least 3 h until the doubling time appeared constant. The pBAD promoter of the pBAD33 derivatives was induced by arabinose (0.2%) at an OD$_{600}$ of ≈0.3 (red arrow). The P$_{A1/O4/O3}$ promoter of the pEG25-derived plasmids was induced by the addition of IPTG (200 μM; green arrow) 1.5 h later. Data points represent mean values from at least two independent experiments, and error bars indicate standard deviations.

The best-conserved stretch of amino acids between GltX and TrpS are the highly conserved KLS[239]KR/KMS[197]KS flexible-loop motifs (Fig. S7). Lys237 and Lys195 participate in the catalytic reaction by stabilizing the transition state of ATP, and intact loop motifs are required for catalysis (37). The observation that HipA phosphorylates GltX at S239 (11) raised the possibility that HipT phosphorylates TrpS at the homologous S197. To test this, we introduced two amino acid changes, S197A and S197D, into TrpS, the latter to mimic a phosphorylated serine. Both changes abolished phosphorylation of HipT$_{O127}$, consistent with the proposal that HipT phosphorylates TrpS at S197 (Fig. 3C). Finally, mass-spectrometric analysis revealed that, indeed, HipT$_{O127}$ phosphorylates TrpS at S197 *in vitro* (Table 1). We also note that HipA did not phosphorylate TrpS (Fig. 3A, lanes 6 and 9), while HipT$_{O127}$ did not phosphorylate GltX (Fig. 3B, lanes 5 and 8). This lack of cross-reactivity in the *in vitro* reactions is consistent with the specificity of the multicopy suppression data.
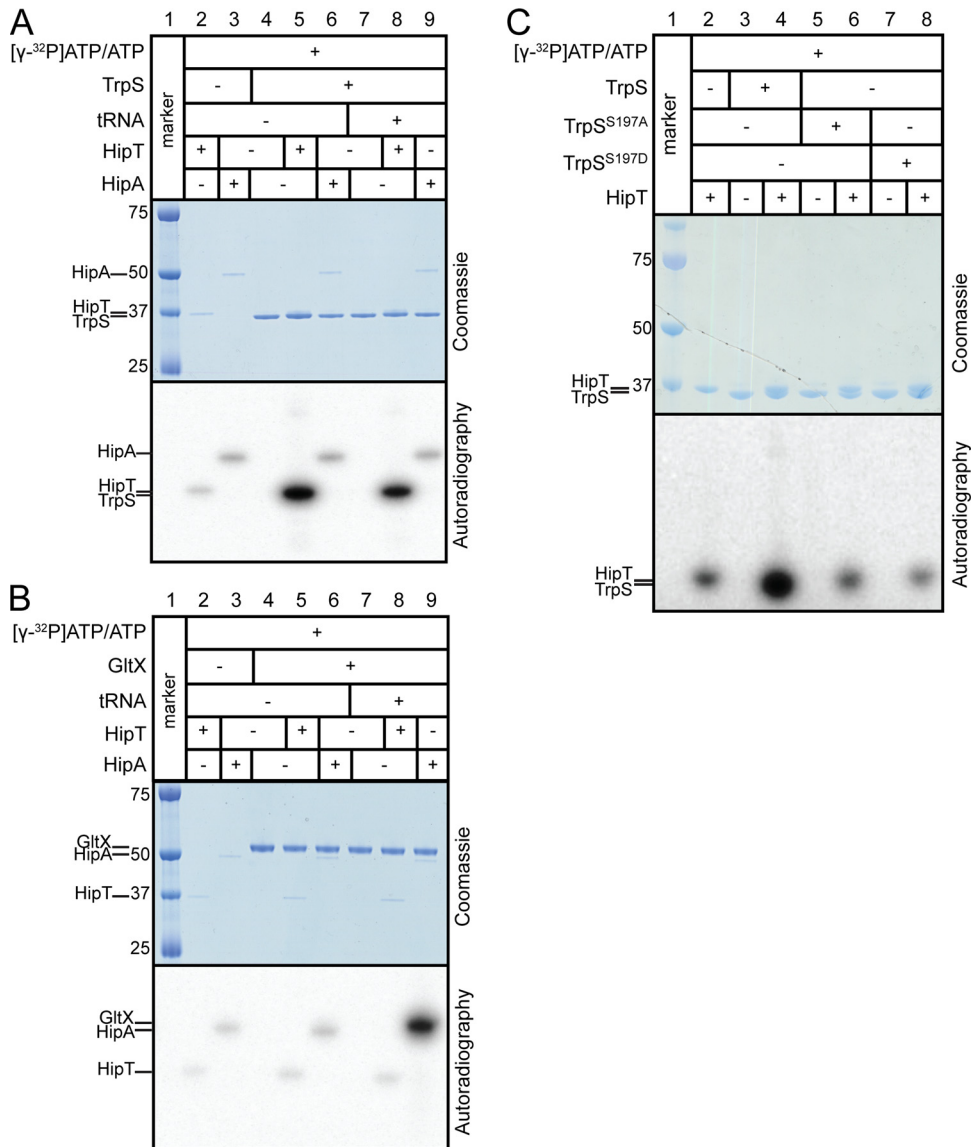
FIG 3 HipT$_{O127}$ phosphorylates TrpS at S197 *in vitro*, and HipT$_{O127}$ is autophosphorylated *in vitro*. (A) Phosphorylation of TrpS and autophosphorylation of HipT$_{O127}$ and HipA *in vitro*. HipT$_{O127}$ or HipA (0.2 μM), [γ-^{32}P]ATP (0.1 μM), and ATP (66 μM) were incubated with (+) or without (−) TrpS [purified from strain C41(DE3)/pSVN46], as well as with (+) or without (−) a mixture of all *E. coli* tRNAs (0.5 μg) per microliter of reaction mixture as indicated. (B) Phosphorylation of GltX and autophosphorylation of HipT$_{O127}$ and HipA *in vitro*. HipT$_{O127}$ or HipA (0.2 μM), [γ-^{32}P]ATP (0.1 μM), and ATP (66 μM) were incubated with (+) or without (−) GltX (purified from strain JW2395), as well as with (+) or without (−) a mixture of *E. coli* tRNAs (0.5 μg) per microliter of reaction mixture as indicated. (C) Phosphorylation of TrpS at S197 and autophosphorylation of HipT$_{O127}$ *in vitro*. HipT$_{O127}$ (1.5 μM) [purified from strain C41(DE3)/pSVN42] was added to the reaction mixtures as indicated, in addition to [γ-^{32}P]ATP (0.1 μM) and ATP (66 μM) with (+) or without (−)TrpS (1.5 μM), TrpS^{S197A} (1.5 μM), or TrpS^{S197D} (1.5 μM) as indicated.

HipA is known to inactivate itself by *trans* autophosphorylation at Ser150 (35, 38). In the reaction mixture containing only HipT$_{O127}$, a faint radioactive band corresponding to the MW of HipT$_{O127}$ was observed (Fig. 3A and B, lane 2). Since HipT$_{O127}$ was the only protein in the reaction mixture, we infer that HipT$_{O127}$ phosphorylates itself. Consistently, the weak HipT$_{O127}$ band also appeared when HipT$_{O127}$ was mixed with the noncognate target GltX (Fig. 3B, lanes 5 and 8). Accordingly, the analysis of the products of the *in vitro* reaction between HipT$_{O127}$ and TrpS by mass spectrometry showed that HipT$_{O127}$ autophosphorylates either on S57 or S59 (Table 1).

HipT$_{O127}$ stimulates production of (p)ppGpp. We and others showed previously that HipA activates RelA to synthesize (p)ppGpp (11, 31, 32). Here, we measured

TABLE 1 Phosphorylation sites identified by LC-MS/MS analysis of products of *in vitro* phosphorylation reaction between HipT$_{O127}$ and TrpS

Protein	Amino acid	Andromeda score	Localization probability	Mass error (ppm)	Phosphopeptide sequence of the best localized MS/MS spectrum
HipT	S57	104.24	0.999992	0.93417	GMS(1)ISGYQPK
HipT	S59	139.32	0.999224	0.14379	GMS(0.001)IS(0.999)GYQPK
TrpS	S197	304.44	0.999903	−0.17001	KMS(1)KSDDNRNNVIGLLEDPK
TrpS	S199	309.72	0.864936	−0.094932	SGARVMSLLEPTKKMS(0.135)KS(0.865)DDNRNNVIGLLEDPK

whether induction of *hipT$_{O127}$* induces (p)ppGpp synthesis and compared it to the effect of induction of *hipA* or *relE* of *E. coli* K-12, the latter of which inhibits translation by ribosome-dependent mRNA cleavage (8). Indeed, induction of both *hipT$_{O127}$* and *hipA* resulted in increased levels of (p)ppGpp, albeit at a somewhat lower level in the case of *hipT$_{O127}$* (Fig. 4A and B). The latter observation is consistent with the fact that tryptophan is encoded by one codon only, compared to two in the case of glutamate, and the fraction of tryptophanyl-tRNA is less than 2% of total tRNA, whereas that of glutamyl-tRNA is more than 7% (39). Thus, deficiency of charged tRNA^{Glu} leads to a higher level of hungry ribosomal A sites and, therefore, a higher number of activated RelA molecules and a higher level of (p)ppGpp. Consistent with previous results (40),
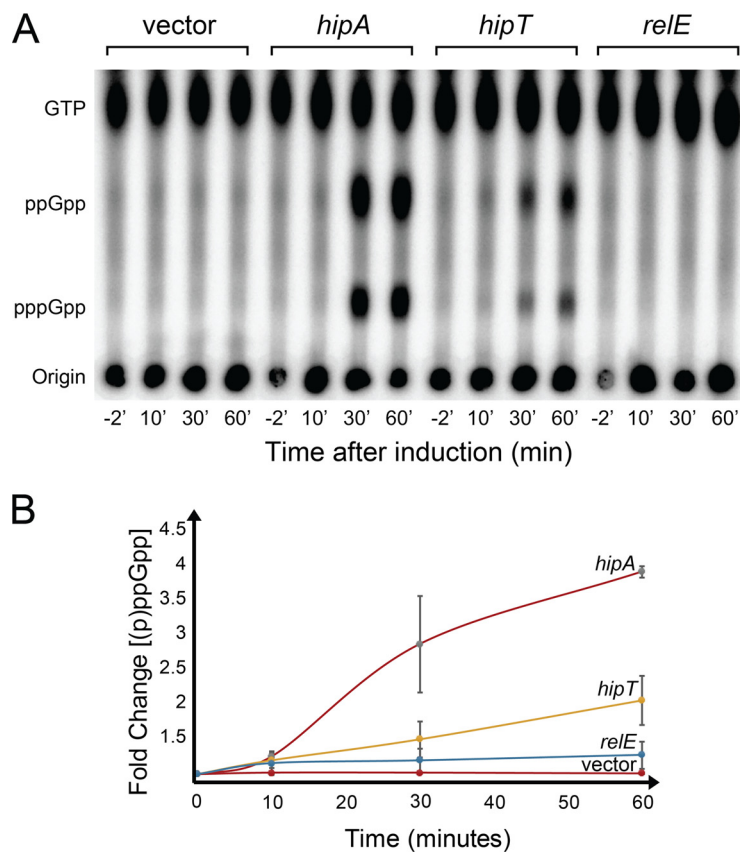

FIG 4 HipT$_{O127}$ induces (p)ppGpp accumulation *in vivo*. Levels of (p)ppGpp of *E. coli* MG1655 containing pNDM220 (vector), pAH1 (pNDM220::*hipA*), pSVN116 (pNDM220::*hipT$_{O127}$*), or pAH2 (pNDM220::*relE*). The toxin-encoding genes were located downstream from the IPTG-inducible P$_{A1/O3/O4}$ promoter (56, 57). (A) Cells were grown exponentially at 37°C in low-phosphate MOPS (morpholinepropanesulfonic acid) minimal medium containing radiolabeled H$_3$^{32}PO$_4$ (see Materials and Methods). Samples were withdrawn before and 10, 30, and 60 min after the addition of IPTG (1 mM) and analyzed by thin-layer chromatography (TLC) and phosphor imaging. (B) Quantification of the results of experiment shown in panel A and of repetitions of the experiment shown in Fig. S8. Materials and Methods gives additional experimental details. Error bars indicate standard deviations of three independent experiments.

induction of *relE* did not stimulate (p)ppGpp synthesis, showing that inhibition of translation *per se* is not sufficient to stimulate (p)ppGpp accumulation (Fig. 4A and B).

DISCUSSION

In this paper, we describe the discovery of a novel family of bacterial serine/ threonine kinases, HipT kinases, that exhibit sequence similarity with HipA of *E. coli* K-12. HipA inhibits GltX (glutamyl-tRNA synthetase) by phosphorylation and thereby triggers RelA-dependent synthesis of (p)ppGpp (11, 31, 32). We found that HipT of *E. coli* O127 phosphorylates and inhibits TrpS (tryptophanyl-tRNA synthetase) and thereby, similarly to HipA, stimulates synthesis of (p)ppGpp (Fig. 4). Even though TrpS and GltX belong to the same class of tRNA synthetases (41), $HipT_{O127}$ and HipA do not exhibit cross-phosphorylation of TrpS and GltX *in vitro*, implying that the two kinases exhibit substrate specificity (Fig. 3A and B). We showed previously that HipA phosphorylates S239 of the conserved $KLS^{239}KR$ motif in GltX (11). A variant of this motif ($KMS^{197}KS$) is present in TrpS. Even though there are two amino acid differences between the two motifs, they represent the overall highest degree of sequence similarity between the two synthetases, suggesting that HipT phosphorylates S197 of TrpS. Indeed, this proposal was confirmed by our mass spectrometric and mutational analysis of TrpS (Table 1 and Fig. 3C).

We showed previously that phosphorylation of the conserved S239 of GltX by HipA requires the presence of $tRNA^{Glu}$ in the *in vitro* reaction mixture (11). We proposed that the binding of $tRNA^{Glu}$ to GltX would induce a conformational change of the motif $KLS^{239}KR$ that would make S239 accessible to phosphorylation (11). In contrast, even though GltX and TrpS belong to the same class of tRNA synthetases and the structural organization of their active sites is similar (42), phosphorylation of TrpS by $HipT_{O127}$ does not require the addition of tRNA (Fig. S6 in the supplemental material). We believe that this difference is consistent with the requirement of GltX for the presence of cognate tRNA to activate glutamate to glutamyl-adenylate (41), a property shared with only two other type I tRNA synthetases (GlnRS and ArgRS). Thus, TrpS does not require the presence of $tRNA^{Trp}$ to activate tryptophan to tryptophanyl-adenylate and does not require $tRNA^{Trp}$ to be phosphorylated by HipT (Fig. S6).

HipA inactivates itself by autophosphorylation at the fully conserved, essential S150 located adjacent to the P loop of the kinase (35). Structural analysis revealed that autophosphorylation stabilizes a conformation of HipA that disrupts the ATP-binding pocket. It was proposed that autophosphorylation of HipA functions in the resuscitation of cells inhibited by HipA by preventing further activity of available toxins. This explanation is plausible, because cells inhibited by HipA somehow must revert the inhibition of GltX before the cells can resuscitate. We observed that $HipT_{O127}$ is autophosphorylated *in vitro* (Fig. 3A and B) at the fully conserved S57 adjacent to the P-loop motif in HipT and, to a minor extent, at S59 in the P-loop motif, both of which are likely to inactivate the enzyme (Table 1).

The *hipT* gene is the third gene of the *hipBST* operon, and HipS and HipT exhibit sequence similarity with either end of HipA. The most parsimonious explanation as to how this arrangement appeared seems to be that *hipA* was duplicated during evolution and split into *hipS* and *hipT*, shifting the kinase specificity during this evolutionary trajectory. Analysis of the structure of HipBA reveals that HipS likely corresponds to the N-terminal subdomain of HipA, which was found to be involved in dimerization during DNA binding, as well as to harbor several mutations associated with high-persister phenotypes (Fig. S9A and B, blue) (26). A more detailed look at the N-terminal subdomain of HipA shows that residues involved in forming the hydrophobic core of the domain are well conserved in HipS, suggesting that HipS and the N-terminal subdomain of HipA share structure, while residues that are involved in HipA-HipA dimerization appear to differ in HipS while being conserved between HipS orthologs. This could suggest that the higher-order structure of HipBST differs from that of HipBA. We also note that several of the known high-persister mutations found in the N-terminal subdomain of HipA (including one of the mutations responsible for the
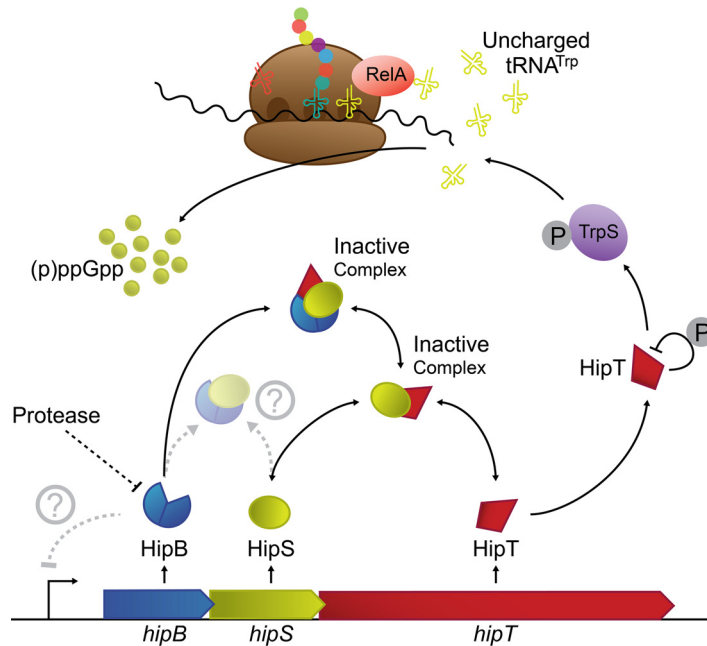
FIG 5 Schematic overview of the components encoded by *hipBST* and their interaction. Our evidence supports the idea that HipT inactivates TrpS by phosphorylation and that HipT phosphorylates itself. Inactivation of TrpS, in turn, increases the level of uncharged tRNA^{Trp} that, in complex with RelA, loads at hungry ribosomal A sites loaded with tryptophan codons. Loading of the binary RelA-tRNA^{Trp} complex at an A site activates RelA to synthesize (p)ppGpp (33). The function of HipT autophosphorylation is unknown, but it may play a role in the resuscitation of HipT-induced persister cells. Furthermore, our data show that the HipBST proteins form one or more complexes and that HipT is inactivated by HipS. HipB contains an HTH DNA-binding motif and probably autoregulates the *hipBST* operon. Speculative interactions are indicated by stippled lines.

hipA7 genotype) are naturally present in HipS, which raises the possibility that HipS is HipA7-like (Fig. S9C). Finally, the structural analysis also reveals that HipB (of HipBST) closely matches the corresponding antitoxin HipB in HipBA and likely harbors a DNA-binding domain (Fig. S9A and B). Of the three proteins, the function of HipS as the "third TA component" is clearly the most intriguing. We found that all three HipS orthologs investigated are able to counteract cognate HipT toxins on their own, while the HipB proteins do not have such an effect (Fig. 1). However, in two cases, we observed that the HipB proteins augmented HipS-mediated neutralization of HipT, suggesting that HipB somehow increases the activity of HipS, for example, by increasing HipS metabolic stability or by stabilizing the HipS-HipT interaction. The latter proposal is consistent with the observation that HipBST form a stable complex *in vivo* (Fig. S4). A summary of our findings is presented in Fig. 5 and described further in the legend to the figure.

Although two-component TA modules are by far the most common, a number of other three-component TA modules have been identified (1). In many of these cases, two adjacent genes exhibit sequence similarity with known type II TA modules, while the function of the third component often remains unclear. However, in a few cases, the function of the third component is known. For example, *M. tuberculosis* contains a three-gene TA module that encodes a RelE-homologous HigB toxin and the HigA antitoxin. The third gene encodes a SecB-like chaperone that controls the stability of HigA such that the antitoxin becomes metabolically unstable under environmental stress, thereby leading to activation of HigB and inhibition of translation by mRNA cleavage (43). Thus, in this TA module, the third component provides a link between cellular physiology and activation of the TA module. ω-ε-ζ of *Streptococcus pyogenes* is a three-component TA module in which ω is a DNA-binding autorepressor of the operon and ε is an antitoxin that neutralizes the ζ toxin by direct protein-

protein contact (44). In the *paaR-paaA-parE* modules of *E. coli* O157:H7, the first gene encodes a transcriptional regulator of the module operon and the second a type II antitoxin that counteracts the activity of the ParE toxin (45). Thus, our work presented here reveals a novel type of three-component TA modules with unknown regulator properties that will be important and exciting to study. We hope that future biochemical and structural studies will be helpful in revealing the mechanisms of HipBST activation and regulation, as well as why this locus is configured as a three-component TA module.

MATERIALS AND METHODS

Strains, plasmids, media, and growth conditions. Strains and plasmids are listed in Table 2, and DNA oligonucleotides in Table 3. Cultures were grown at 37°C with shaking at 160 rpm in Luria-Bertani (LB) medium. When required, the medium was supplemented with 25 μg/ml chloramphenicol, 30 μg/ml or 100 μg/ml ampicillin, and 25 μg/ml kanamycin. Gene expression from plasmids carrying the pBAD promoter was induced by 0.2% arabinose and repressed by 0.2% glucose. Gene expression from plasmids carrying the synthetic $P_{A1/O4/O3}$ promoter was induced by 200 μM isopropyl β-D-1 thiogalactopyranoside (IPTG). The solid medium used to grow cells was Luria-Bertani agar (LB agar) medium supplemented with the appropriate antibiotics and incubated at 37°C for approximately 16 h unless otherwise stated.

Gene knockout by P1 transduction. To construct strain *E. coli* MG1655Δ*ydeA*, gene knockout was obtained by phage P1 transduction using a strain of the Keio collection as donor according to standard procedure (46, 47).

Multicopy suppression screening. Genomic DNA (gDNA) of *E. coli* MG1655Δ*ydeA* was purified according to the manufacturer's instructions (EdgeBio). The gDNA was then partially digested with Sau3AI (Bsp143I) and fragments inserted into pBR322, which had been digested with BamHI and dephosphorylated. The gene library was transformed into a strain harboring the pBAD33::*hipT*$_{O127}$ plasmid and plated on agar plates containing arabinose.

Site-directed mutagenesis. Amino acid changes TrpS^{S197A}, TrpS^{S197D}, and HipT$_{O127}$^{D233Q} were constructed by PCR mutagenesis (Table 3). The PCR products were digested with DpnI, and the resulting plasmids were transformed into *E. coli* strain DH5α.

Protein purification. HipT$_{O127}$ (produced by pSVN42) was purified from *E. coli* strain BL21 that also produced HipB$_{O127}$ and HipS$_{O127}$ (pSVN44). Overnight cultures were diluted 100-fold into 350 ml fresh LB medium. At an optical density at 600 nm (OD$_{600}$) of $\approx$0.3, the toxin gene was induced by the addition of 1 mM IPTG for 4 h, and cells were harvested by centrifugation. Pellets were resuspended in 25 ml cold buffer A (50 mM NaH$_2$PO$_4$ [pH 8], 0.3 M NaCl, 10 mM imidazole, 5 mM β-mercaptoethanol [BME]) with the addition of half a protease inhibitor cocktail each. Cells were carefully sonicated for 5 min at 60% amplification (2 s on and 2 s off) while still kept cold. The cell lysate was spun at 16,000 rpm for 30 min at 4°C, and the cleared lysate was incubated at 4°C for 1 h with 1 ml Ni beads that had been freshly equilibrated in the same buffer for 1 h. Protein-bound beads were then applied to gravity flow columns and washed with 50 ml of buffer B (50 mM NaH$_2$PO$_4$ [pH 8], 0.3 M NaCl, 35 mM imidazole, 1 mM BME). As described previously, the toxin and antitoxins were separated with urea washes to leave the His-tagged protein on the affinity column (48). His-tagged proteins were purified according to the manufacturer's protocol, further purified using an Äkta Pure (GE Healthcare) fast protein liquid chromatography (FPLC) instrument, and stored in 200 mM NaCl, 50 mM Tris-HCl, and 5% glycerol. All proteins purified with His tags were tested and compared to wild-type proteins *in vivo* prior to purification in order to assess their functionality.

Phosphorylation *in vitro*. Phosphorylation reactions were performed in the presence of 0.05 μl [γ-^{32}P]ATP (6,000 Ci/mmol; Perkin Elmer) per microliter of reaction mixture, 66.6 μM ATP (nonradioactive), and aminoacylation buffer (1 mM dithiothreitol [DTT], 10 mM KCl, 16 μM ZnSO$_4$, and 20 mM MgCl$_2$) for 45 min as described previously (11). Each reaction was stopped by the addition of 1 volume Laemmli loading buffer, the reaction mixture was incubated for 10 min at 95°C, and proteins were resolved by SDS-PAGE and exposed using phosphorimaging (GE Healthcare) overnight.

Phosphorylation *in vitro* measured by LC-MS. The phosphorylation reaction was performed with 13.5 μM TrpS and 6.7 μM HipT$_{O127}$ in the presence of 5 mM ATP and aminoacylation buffer for 45 min at 37°C. The reaction was stopped by the addition of 4 volumes of denaturation buffer (6 M urea, 2 M thiourea, 1 mM DTT, and 10 mM Tris-HCl, pH 8.0), and the reaction mixture incubated for 30 min at room temperature, followed by incubation with 5.5 mM iodoacetamide for 45 min at room temperature. Denatured proteins were digested overnight either with endoproteinase Lys-C (1:100 [wt/wt]; Wako) in 20 mM bicarbonate, pH 8.0, or with endoproteinase Arg-C (1:100 [wt/wt]; Roche) in 90 mM Tris-HCl, pH 7.6, 8.5 mM CaCl$_2$, 5 mM DTT, 0.5 mM EDTA. Digested peptides were purified via Pierce C18 Spin Tips, and 0.5 μg of each sample was measured by liquid chromatography-tandem mass spectrometry (LC-MS/MS) as described previously (49). Briefly, peptides were separated by an Easy-nL 1200 ultra-high-performance liquid chromatography (UHPLC) instrument (Thermo Fisher Scientific) and transferred into an online coupled Q Exactive HF mass spectrometer (Thermo Fisher Scientific) by nanoelectrospray ionization. Peptides were eluted from a 20-cm-long analytical column packed with 1.9-μm reverse-phase particles using a 33-min segmented gradient of 5% to 50% solvent B (80% [vol/vol] acetonitrile, 0.1% [vol/vol] formic acid) at a constant flow rate of 300 nl/min. Full-scan MS spectra were acquired in a mass range from 300 to 1,650 *m/z* with a maximum injection time of 45 ms and a resolution of 60,000. Higher-energy collisional dissociation MS/MS scans of the 7 (Top7 data-dependent method) most abundant peaks were

TABLE 2 Bacterial strains and plasmids

Strain or plasmid	Description[a]	Reference or source
E. coli strains		
MG1655	Wild-type K-12	58
MG1655Δ*ydeA*	K-12 MG1655Δ*ydeA*::FRT	This work
BL21	F⁻ *ompT hsdS*_B (r_B⁻ m_B⁻) *gal dcm*	59
C41 (DE3)	Derived from BL21(DE3): F⁻ *ompT hsdS*_B (r_B⁻ m_B⁻) *gal dcm* (DE3)	60
EG235	C41 (DE3) Δ*hipBA*::*kan*, pMG25::*gltX* (optimized SD), pBAD33::His₆::*hipA* (SD8 and start codon ATG)	Laboratory collection
JW2395	AG1 [*recA1 endA1 gyrA96 thi-1 hsdR17 supE44 relA1*] carrying pCA24N::*gltX*, GltX purification plasmid encoding N-terminally His₆-tagged *gltX*, from ASKA collection	55
Plasmids		
pBAD33	p15 *araC* P_{BAD}, Cm^r	61
pNDM220	Mini-R1 *lacI*^q P_{A1/O4/O3}, Amp^r	56
pCP20	pSC101 *rep*(Ts), Amp^r Cm^r	47
pBR322	pMB1 *rop*, Amp^r Tet^r	62
pMG25	pUC *lacI*^q P_{A1/O4/O3}, Amp^r	Laboratory collection
pEG25	pMG25 derivative that has reduced leakiness of the IPTG-inducible P_{A1/O4/O3} promoter	Laboratory collection
pEG::*gltX*	pMG25::*gltX*, optimized SD	Laboratory collection
pEG::_{His6}*hipA*	pBAD33::_{His6}*hipA* purification plasmid harboring N-terminally His₆-tagged *hipA*	Laboratory collection
pET-15b	pBR322 *lacI* P_{T7}, Amp^r	Novagen
pKG127	pUC57::*hipBST*_{O127}	Genscript
pSVN1	pBAD33::*hipT*_{O127}, start codon GTG	This work
pSVN42	pEG25::*hipT*_{O127::His6}, optimized SD, HipT_{O127} purification plasmid C-terminally His₆-tagged *hipT*_{O127}	This work
pSVN46	pEG25::*trpS*_{His6}, optimized SD, TrpS purification plasmid harboring C-terminally His₆-tagged *trpS*	This work
pSVN49	pEG25::*trpS*^{S197D}_{His6}, optimized SD, TrpS^{S197D} purification plasmid harboring C-terminally His₆-tagged *trpS*^{S197D}	This work
pSVN52	pEG25::*trpS*^{S197A}_{His6}, optimized SD, TrpS^{S197A} purification plasmid harboring C-terminally His₆-tagged *trpS*^{S197A}	This work
pSVN60	pUC57::_{His6-TEV}*hipB*::*hipS*::*hipT*_{O127}, optimized SDs for all genes	Genscript
pSVN61	pUC57::*hipB*::*hipS*::*hipT*_{O127::His6}, optimized SDs for all genes used for TA complex purification via C-terminally His₆-tagged *hipT*_{O127}	Genscript
pSVN37	pEG25::*trpS*, optimized SD	This work
pSVN44	pBAD33::*hipBS*_{O127}, optimized SD for *hipB*_{O127}	This work
pSVN94	pET-15b::_{His6-TEV}*hipB*::*hipS*::*hipT*^{D233Q}_{O127}, optimized SDs for all genes	This work
pSVN103	pNDM220::*trpS*, optimized SD	This work
pSVN109	pNDM220::*hipS*_{O127}, optimized SD	This work
pSVN110	pNDM220::*hipBS*_{O127}, optimized SDs	This work
pSVN111	pNDM220::*hipB*_{O127}, optimized SD	This work
pSVN113	pUC57::*hipBST*_{Hi}	Genscript
pSVN114	pUC57::*hipBST*_{Ta}	Genscript
pSVN116	pNDM220::*hipT*_{O127}, start codon GTG	This work
pSVN122	pNDM220::*hipB*_{Hi}, optimized SD	This work
pSVN123	pNDM220::*hipS*_{Hi}, optimized SD	This work
pSVN124	pNDM220::*hipBS*_{Hi}, optimized SD for *hipB*_{Hi}, overlapping *hipB*_{Hi} and *hipS*_{Hi}	This work
pSVN126	pNDM220::*hipB*_{Ta}, optimized SD	This work
pSVN127	pNDM220::*hipS*_{Ta}, optimized SD	This work
pSVN128	pNDM220::*hipBS*_{Ta}, optimized SD for *hipB*_{Ta}, overlapping *hipB*_{Ta} and *hipS*_{Ta}	This work
pSVN129	pBAD33::*hipT*_{Ta}, optimized SD, start codon GTG	This work
pSVN135	pBAD33::*hipT*_{Hi}, optimized SD	This work
pSVN138	pNDM220::*hipBS*_{Ta}, optimized SDs	This work
pSVN139	pNDM220::*hipBS*_{Hi}, optimized SDs	This work
pAH1	pNDM220::*hipA*	A. Harms
pAH2	pNDM220::*relE*	A. Harms

[a]SD, Shine-Dalgarno sequence.

recorded with a maximum injection time of 220 ms at a resolution of 60,000. Acquired raw data were processed with MaxQuant software (version 1.5.2.8) (50) using default settings if not stated otherwise. The derived peak list was searched against a reference *E. coli* K-12 proteome (Taxon identifier 83333) containing 4,324 entries (UniProt, release 2017/12), the protein sequence of HipT, HipS, and HipB from *E. coli* O127:H6, and a file containing 245 common laboratory contaminants using a built-in Andromeda search engine (51). Methionine oxidation, protein N-terminal acetylation, and Ser/Thr/Tyr phosphorylation were defined as variable modifications, and carbamidomethylation of cysteines was set as a fixed modification. The maximum number of missed cleavages allowed was set to 3 for the endoproteinase Lys-C and to 2 for Arg-C. Only phosphopeptides with an Andromeda score of >70 and a localization probability of >0.75 were considered, and their MS/MS spectra were inspected manually (Fig. S10).

Measurement of cellular (p)ppGpp levels. Measurement of cellular (p)ppGpp levels was performed as described previously (52, 53).

TABLE 3 Oligonucleotides

Oligonucleotide	Sequence
FP1(GTG)	CCCCCGTCGACGGATCCAAGGAGTTTTATAAGTGGCGAATTGTCGTATTCTG
RP1	CCCCCGCATGCGAATTCGCTCACAGCAGCCCCAGACG
FP25	CCCCCTCGAGGGATCCAAAATAAGGAGGAAAAAAAAATGATCTGCTCAGGACCAC
RP15	GGGGGAATTCAAGCTTTCACTCGCCGATGCATAG
FP22	CCCCCTCGAGGGATCCAAAATAAGGAGGAAAAAAAAATGCATCGGCGAGTGAAAG
RP14	GGGGGAATTCAAGCTTTTATTCCTCCCAAGGTAAAATC
FP39	CCCCGGGGGATCCAAAATAAGGAGGAAAAAAAAATGAATTTTTGTCGTATTTTATTAAAG
RP21	GGGGGTACCCTGCAGTTATAGTTCAGGTTCATTTAATAG
FP29	CCCCCGGGGGATCCAAAATAAGGAGGAAAAAAAAATGGACAATCTTAGTGCAC
RP19	GGGGGTACCCTGCAGCTAAATCGCGCATAGTGAAAC
FP30	CCCCCGGGGGATCCAAAATAAGGAGGAAAAAAAAATGCGCGATTTAGTCCGC
RP20	GGGGGTACCCTGCAGTCATTGTTTTTCTTCCTG
FP42	AAAATAAGGAGGAAAAAAAAATGCGCGATTTAGTCCG
RP30	TTTTTTTTCCTCCTTATTTTCTAAATCGCGCATAGTGAAAC
FP34	CCCCCGGGGGATCCAAAATAAGGAGGAAAAAAAAGTGGACCGTTGTCTGATCAC
RP24	GGGGGTACCCTGCAGTTACCGGTCGAGATCGACAAC
FP32	CCCCCGGGGGATCCAAAATAAGGAGGAAAAAAAAATGAGCCATAGAAATCTACTCG
RP22	GGGGGTACCCTGCAGTTACTTTGCGGCCCATAACTTG
FP33	CCCCCGGGGGATCCAAAATAAGGAGGAAAAAAAAATGGGCCGCAAAGTAATTG
RP23	GGGGGTACCCTGCAGTTAATCATTAACCTCAAG
FP41	AAAATAAGGAGGAAAAAAAAATGGGCCGCAAAGTAATT
RP29	TTTTTTTTCCTCCTTATTTTCTATTTGGCGGCCCATAACTTGATAC
trpS Fw	CCCCCGGATCCAAAATAAGGAGGAAAAAAAAATGACTAAGCCCATCG
trpS RP4	GGGGGAATTCTTACGGCTTCGCCACAAACC
trpS Rv	CCCCCAAGCTTTTACGGCTTCGCCACAAAC
FP13	CCCCGGATCCAAAATAAGGAGGAAAAAAAAATGGCGAATTGTCGTATTC
RP5	GGGGGAAGCTTTCAGTGATGGTGATGGTGATGCAGCAGCCCCAGACGATG
trpS RP3	GGGGGAAGCTTTTAGTGATGGTGATGGTGATGCGGCTTCGCCACAAACC
trpS S197A Fw	AGAAGATGGCCAAGTCTGACGATAATCGC
trpS S197A Rv	AGACTTGGCCATCTTCTTGGTCGGCTC
trpS S197D Fw	AGAAGATGGACAAGTCTGACGATAATCGCA
trpS S197D Rv	CAGACTTGTCCATCTTCTTGGTCGGCTC
FP5	CCCCCGTCGACGGATCCAAGGAAAAAAAAAGTGGCGAATTGTCGTATTCTG
FP15	CCCCGTCGACAAAATAAGGAGGAAAAAAAAATGATCTGCTCAGGACCA
RP6	GGGGGCATGCTTATTCCTCCCAAGGTAAAA
hipX D233Q Fw	CGGTGTATCAGTTTGTTTCTGTCGCTCCC
hipX D233Q Rv	GAAACAAACTGATACACCGGCGCTAACG
FP16	CCCCGAATTCAAAATAAGGAGGAAAAAAAAATGCATCACCATCACCATCACGAAAACCTGTACTTCCAAGGGATCTGCTCAGGACCACAAAATC
RP7	GGGGAAGCTTTCACTCGCCGATGCATAGTTTC
RP13	GGGGGAATTCAAGCTTTTAGTGATGGTGATGGTGATGTTCCTCCCAAGGTAAAATC

Mass spectrometry. The mass spectrometry proteomics data have been deposited to the ProteomeXchange Consortium via the PRIDE (54) partner repository with the data set identifier PXD012023.

Construction of plasmids. Construction of plasmids is summarized below.

pKG127. The region of the *E. coli* O127 E2348/69 genome (accession number NC_011601.1) containing the *hipBST* locus (+3,948,403 to +3,950,320) was synthesized (GeneScript) and inserted into the SalI restriction site of pUC57.

pSVN1. *hipT*$_{O127}$ with start codon GTG was amplified from pKG127 using primers FP1(GTG) and RP1. The resulting PCR product was digested with SalI and SphI and ligated with pBAD33.

pSVN37. *trpS* was amplified from pCA24N::*trpS* from the ASKA collection (55) using primers trpS Fw and trpS Rv. The resulting PCR product was digested with BamHI and HindIII and ligated into pEG25.

pSVN42. *hipT*$_{O127::His6}$ was amplified from pKG127 using primers FP13 and RP5. The resulting PCR product was digested with BamHI and HindIII and ligated into pEG25.

pSVN44. *hipBS*$_{O127}$ was amplified from pKG127 using primers FP15 and RP6. The resulting PCR product was digested with SalI and SphI and ligated into pBAD33.

pSVN46. *trpS*$_{His6}$ was amplified from pSVN37 using primers trpS Fw and trpS RP3. The resulting PCR product was digested with BamHI and HindIII and ligated into pEG25.

pSVN49. The mutation in *trpS*^{S197D}$_{His6}$ was created using pSVN46 and primers trpS S197D Fw and trpS S197D Rv in a site-directed plasmid mutagenesis PCR. The fragment was digested with DpnI before being transformed into *E. coli* DH5α.

pSVN52. The mutation in *trpS*^{S197A}$_{His6}$ was created using pSVN46 and primers trpS S197A Fw and trpS S197A Rv in a site-directed plasmid mutagenesis PCR. The fragment was digested with DpnI before being transformed into *E. coli* DH5α.

pSVN94. $_{His6-tev}$*hipB*$_{O127}$::*hipS*$_{O127}$::*hipT*$_{O127}$ with optimized SDs for all three genes was subcloned from pSVN60 by digesting with XbaI and XhoI, purifying the DNA fragment from a 1% agarose gel, and ligating into pET-15b. The mutation in $_{His6-tev}$*hipB*$_{O127}$::*hipS*::*hipT*^{D233Q} was created using primers hipX D233Q Fw

and hipX D233Q Rv in a site-directed plasmid mutagenesis PCR. The fragment was digested with DpnI before transformation.

pSVN103. $trpS$ was amplified from pCA24N::$trpS$ from the ASKA collection (55) using primers trpS Fw and trpS RP4. The resulting PCR product was digested with BamHI and EcoRI and ligated into pNDM220.

pSVN109. $hipS_{O127}$ was amplified from pKG127 using primers FP22 and RP14. The resulting PCR product was digested with XhoI and EcoRI and ligated into pNDM220.

pSVN110. $hipBS_{O127}$ was amplified from pSVN61 using primers FP25 and RP14. The resulting PCR product was digested with XhoI and EcoRI and ligated into pNDM220.

pSVN111. $hipB_{O127}$ was amplified from pSVN61 using primers FP25 and RP15. The resulting PCR product was digested with XhoI and EcoRI and ligated into pNDM220.

pSVN113. The region of the *H. influenzae* Rd KW20 genome (NC_000907.1) containing the *hipBST* locus (+710,585 to +712,589) was synthesized and inserted into the SalI site of pUC57 (GeneScript).

pSVN114. The region of the *Tolumonas auensis* DSM 9187 genome (NC_012691.1) containing the *hipBST* locus (+2,117,168 to +2,119,170) was synthesized and inserted into the SalI site of pUC57 (GeneScript).

pSVN116. $hipT_{O127}$ was amplified using primers FP5 and RP1 from pSVN1. The fragment was then cloned into cut pNDM220 using BamHI and EcoRI, resulting in pSVN116 (pNDM220::$hipT_{O127}$).

pSVN122. $hipB_{Hi}$ was amplified from pSVN113 using primers FP29 and RP19. The resulting PCR product was digested with BamHI and KpnI and ligated into pNDM220.

pSVN123. $hipS_{Hi}$ was amplified from pSVN113 using primers FP30 and RP20. The resulting PCR product was digested with BamHI and KpnI and ligated into pNDM220.

pSVN124. $hipBS_{Hi}$ was amplified from pSVN113 using primers FP29 and RP20. The resulting PCR product was digested with BamHI and KpnI and ligated into pNDM220.

pSVN126. $hipB_{Ta}$ was amplified from pSVN114 using primers FP32 and RP22. The resulting PCR product was digested with BamHI and KpnI and ligated into pNDM220.

pSVN127. $hipS_{Ta}$ was amplified from pSVN114 using primers FP33 and RP23. The resulting PCR product was digested with BamHI and KpnI and ligated into pNDM220.

pSVN128. $hipBS_{Ta}$ was amplified from pSVN114 using primers FP32 and RP23. The resulting PCR product was digested with BamHI and KpnI and ligated into pNDM220.

pSVN129. $hipT_{Ta}$ was amplified from pSVN114 using primers FP34 and RP24. The resulting PCR product was digested with XmaI and PstI and ligated into pBAD33.

pSVN135. $hipT_{Hi}$ was amplified from pSVN113 using primers FP39 and RP21. The resulting PCR product was digested with XmaI and PstI and ligated into pBAD33.

pSVN138. The optimized SD inserted between $hipB_{Ta}$ and $hipS_{Ta}$ was created using pSVN128 and primers FP41 and RP29 in a site-directed plasmid mutagenesis PCR. Eight reactions were carried out at different temperatures with a gradient PCR. The samples were pooled and digested with DpnI to digest the parental plasmid before being transformed into *E. coli* DH5α.

pSVN139. The optimized SD inserted between $hipB_{Hi}$ and $hipS_{Hi}$ was created using pSVN124 and primers FP42 and RP30 in a site-directed plasmid mutagenesis PCR. The fragment was digested with DpnI before transformation.

SUPPLEMENTAL MATERIAL

Supplemental material for this article may be found at https://doi.org/10.1128/mBio .01138-19.

FIG S1, PDF file, 2.2 MB.
FIG S2, PDF file, 0.4 MB.
FIG S3, PDF file, 0.3 MB.
FIG S4, PDF file, 2.9 MB.
FIG S5, PDF file, 0.2 MB.
FIG S6, PDF file, 1.1 MB.
FIG S7, PDF file, 0.4 MB.
FIG S8, PDF file, 2.7 MB.
FIG S9, PDF file, 0.2 MB.
FIG S10, PDF file, 0.2 MB.

REFERENCES

1. Harms A, Brodersen DE, Mitarai N, Gerdes K. 2018. Toxins, targets, and triggers: an overview of toxin-antitoxin biology. Mol Cell 70:768–784. https://doi.org/10.1016/j.molcel.2018.01.003.

2. Page R, Peti W. 2016. Toxin-antitoxin systems in bacterial growth arrest and persistence. Nat Chem Biol 12:208. https://doi.org/10.1038/nchembio.2044.

3. Hayes F. 2003. Toxins-antitoxins: plasmid maintenance, programmed cell death, and cell cycle arrest. Science 301:1496–1499. https://doi.org/10.1126/science.1088157.

4. Chan WT, Espinosa M, Yeo CC. 2016. Keeping the wolves at bay: antitoxins of prokaryotic type II toxin-antitoxin systems. Front Mol Biosci 3:9. https://doi.org/10.3389/fmolb.2016.00009.

5. Jørgensen MG, Pandey DP, Jaskolska M, Gerdes K. 2009. HicA of Escherichia coli defines a novel family of translation-independent mRNA interferases in bacteria and archaea. J Bacteriol 191:1191–1199. https://doi.org/10.1128/JB.01013-08.

6. Gerdes K. 2000. Toxin-antitoxin modules may regulate synthesis of macromolecules during nutritional stress. J Bacteriol 182:561–572. https://doi.org/10.1128/jb.182.3.561-572.2000.

7. Pandey DP, Gerdes K. 2005. Toxin-antitoxin loci are highly abundant in free-living but lost from host-associated prokaryotes. Nucleic Acids Res 33:966–976. https://doi.org/10.1093/nar/gki201.

8. Pedersen K, Zavialov AV, Pavlov MY, Elf J, Gerdes K, Ehrenberg M. 2003. The bacterial toxin RelE displays codon-specific cleavage of mRNAs in the ribosomal A site. Cell 112:131–140. https://doi.org/10.1016/S0092-8674(02)01248-5.

9. Zhang Y, Zhang J, Hoeflich KP, Ikura M, Qing G, Inouye M. 2003. MazF cleaves cellular mRNAs specifically at ACA to block protein synthesis in Escherichia coli. Mol Cell 12:913–923. https://doi.org/10.1016/S1097-2765(03)00402-7.

10. Winther KS, Gerdes K. 2011. Enteric virulence associated protein VapC inhibits translation by cleavage of initiator tRNA. Proc Natl Acad Sci U S A 108:7403–7407. https://doi.org/10.1073/pnas.1019587108.

11. Germain E, Castro-Roa D, Zenkin N, Gerdes K. 2013. Molecular mechanism of bacterial persistence by HipA. Mol Cell 52:248–254. https://doi.org/10.1016/j.molcel.2013.08.045.

12. Cheverton AM, Gollan B, Przydacz M, Wong CT, Mylona A, Hare SA, Helaine S. 2016. A Salmonella toxin promotes persister formation through acetylation of tRNA. Mol Cell 63:86–96. https://doi.org/10.1016/j.molcel.2016.05.002.

13. Bernard P, Couturier M. 1992. Cell killing by the F plasmid CcdB protein involves poisoning of DNA-topoisomerase II complexes. J Mol Biol 226:735–745. https://doi.org/10.1016/0022-2836(92)90629-X.

14. Jurėnas D, Chatterjee S, Konijnenberg A, Sobott F, Droogmans L, Garcia-Pino A, Van Melderen L. 2017. AtaT blocks translation initiation by N-acetylation of the initiator tRNA(fMet). Nat Chem Biol 13:640–646. https://doi.org/10.1038/nchembio.2346.

15. Miki T, Park JA, Nagao K, Murayama N, Horiuchi T. 1992. Control of segregation of chromosomal DNA by sex factor F in Escherichia coli. Mutants of DNA gyrase subunit A suppress letD (ccdB) product growth inhibition. J Mol Biol 225:39–52. https://doi.org/10.1016/0022-2836(92)91024-J.

16. Jiang Y, Pogliano J, Helinski DR, Konieczny I. 2002. ParE toxin encoded by the broad-host-range plasmid RK2 is an inhibitor of Escherichia coli gyrase. Mol Microbiol 44:971–979. https://doi.org/10.1046/j.1365-2958.2002.02921.x.

17. Freire DM, Gutierrez C, Garza-Garcia A, Grabowska AD, Sala AJ, Ariyachaokun K, Panikova T, Beckham KSH, Colom A, Pogenberg V, Cianci M, Tuukkanen A, Boudehen YM, Peixoto A, Botella L, Svergun DI, Schnappinger D, Schneider TR, Genevaux P, de Carvalho LPS, Wilmanns M, Parret AHA, Neyrolles O. 2019. An NAD(+) phosphorylase toxin triggers Mycobacterium tuberculosis cell death. Mol Cell 73:1282–1291.e8. https://doi.org/10.1016/j.molcel.2019.01.028.

18. Skjerning RB, Senissar M, Winther KS, Gerdes K, Brodersen DE. 2019. The RES domain toxins of RES-Xre toxin-antitoxin modules induce cell stasis by degrading NAD. Mol Microbiol 111:221–236. https://doi.org/10.1111/mmi.14150.

19. Arnoldini M, Mostowy R, Bonhoeffer S, Ackermann M. 2012. Evolution of stress response in the face of unreliable environmental signals. PLoS Comput Biol 8:e1002627. https://doi.org/10.1371/journal.pcbi.1002627.

20. Radzikowski JL, Vedelaar S, Siegel D, Ortega AD, Schmidt A, Heinemann M. 2016. Bacterial persistence is an active sigmaS stress response to metabolic flux limitation. Mol Syst Biol 12:882. https://doi.org/10.15252/msb.20166998.

21. Harms A, Maisonneuve E, Gerdes K. 2016. Mechanisms of bacterial persistence during stress and antibiotic exposure. Science 354:aaf4268. https://doi.org/10.1126/science.aaf4268.

22. Veening JW, Smits WK, Kuipers OP. 2008. Bistability, epigenetics, and bet-hedging in bacteria. Annu Rev Microbiol 62:193–210. https://doi.org/10.1146/annurev.micro.62.081307.163002.

23. Dorr T, Vulic M, Lewis K. 2010. Ciprofloxacin causes persister formation by inducing the TisB toxin in Escherichia coli. PLoS Biol 8:e1000317. https://doi.org/10.1371/journal.pbio.1000317.

24. Goneau LW, Yeoh NS, MacDonald KW, Cadieux PA, Burton JP, Razvi H, Reid G. 2014. Selective target inactivation rather than global metabolic dormancy causes antibiotic tolerance in uropathogens. Antimicrob Agents Chemother 58:2089–2097. https://doi.org/10.1128/AAC.02552-13.

25. Moyed HS, Bertrand KP. 1983. hipA, a newly recognized gene of Escherichia coli K-12 that affects frequency of persistence after inhibition of murein synthesis. J Bacteriol 155:768–775.

26. Schumacher MA, Balani P, Min J, Chinnam NB, Hansen S, Vulić M, Lewis K, Brennan RG. 2015. HipBA–promoter structures reveal the basis of heritable multidrug tolerance. Nature 524:59. https://doi.org/10.1038/nature14662.

27. Korch SB, Henderson TA, Hill TM. 2003. Characterization of the hipA7 allele of Escherichia coli and evidence that high persistence is governed by (p)ppGpp synthesis. Mol Microbiol 50:1199–1213. https://doi.org/10.1046/j.1365-2958.2003.03779.x.

28. Korch SB, Hill TM. 2006. Ectopic overexpression of wild-type and mutant hipA genes in Escherichia coli: effects on macromolecular synthesis and persister formation. J Bacteriol 188:3826–3836. https://doi.org/10.1128/JB.01740-05.

29. Stancik IA, Šestak MS, Ji B, Axelson-Fisk M, Franjevic D, Jers C, Domazet-Lošo T, Mijakovic I. 2018. Serine/threonine protein kinases from Bacteria, Archaea and Eukarya share a common evolutionary origin deeply rooted in the tree of life. J Mol Biol 430:27–32. https://doi.org/10.1016/j.jmb.2017.11.004.

30. Hanks SK, Quinn AM, Hunter T. 1988. The protein kinase family: conserved features and deduced phylogeny of the catalytic domains. Science 241:42–52. https://doi.org/10.1126/science.3291115.

31. Kaspy I, Rotem E, Weiss N, Ronin I, Balaban NQ, Glaser G. 2013. HipA-mediated antibiotic persistence via phosphorylation of the glutamyl-tRNA-synthetase. Nat Commun 4:3001. https://doi.org/10.1038/ncomms4001.

32. Bokinsky G, Baidoo EE, Akella S, Burd H, Weaver D, Alonso-Gutierrez J, García-Martín H, Lee TS, Keasling JD. 2013. HipA-triggered growth arrest and β-lactam tolerance in Escherichia coli are mediated by RelA-dependent ppGpp synthesis. J Bacteriol 195:3173–3182. https://doi.org/10.1128/JB.02210-12.

33. Winther KS, Roghanian M, Gerdes K. 2018. Activation of the stringent response by loading of RelA-tRNA complexes at the ribosomal A-site. Mol Cell 70:95–105.e4. https://doi.org/10.1016/j.molcel.2018.02.033.

34. Schumacher MA, Piro KM, Xu W, Hansen S, Lewis K, Brennan RG. 2009. Molecular mechanisms of HipA-mediated multidrug tolerance and its neutralization by HipB. Science 323:396–401. https://doi.org/10.1126/science.1163806.

35. Schumacher MA, Min J, Link TM, Guan Z, Xu W, Ahn Y-H, Soderblom EJ, Kurie JM, Evdokimov A, Moseley MA, Lewis K, Brennan RG. 2012. Role of unusual P-loop ejection and autophosphorylation in HipA-mediated persistence and multidrug tolerance. Cell Rep 2:518–525. https://doi.org/10.1016/j.celrep.2012.08.013.

36. Edgar RC. 2004. MUSCLE: multiple sequence alignment with high accuracy and high throughput. Nucleic Acids Res 32:1792–1797. https://doi.org/10.1093/nar/gkh340.

37. Sekine S, Nureki O, Dubois DY, Bernier S, Chenevert R, Lapointe J, Vassylyev DG, Yokoyama S. 2003. ATP binding by glutamyl-tRNA synthetase is switched to the productive mode by tRNA binding. EMBO J 22:676–688. https://doi.org/10.1093/emboj/cdg053.

38. Correia FF, D'Onofrio A, Rejtar T, Li L, Karger BL, Makarova K, Koonin EV, Lewis K. 2006. Kinase activity of overexpressed HipA is required for

growth arrest and multidrug tolerance in Escherichia coli. J Bacteriology 188:8360–8367. https://doi.org/10.1128/JB.01237-06.

39. Dong H, Nilsson L, Kurland CG. 1996. Co-variation of tRNA abundance and codon usage in Escherichia coli at different growth rates. J Mol Biol 260:649–663. https://doi.org/10.1006/jmbi.1996.0428.

40. Germain E, Roghanian M, Gerdes K, Maisonneuve E. 2015. Stochastic induction of persister cells by HipA through (p)ppGpp-mediated activation of mRNA endonucleases. Proc Natl Acad Sci U S A 112:5171–5176. https://doi.org/10.1073/pnas.1423536112.

41. Giege R, Springer M. 23 May 2016, posting date. Aminoacyl-tRNA synthetases in the bacterial world. EcoSal Plus 2016 . https://doi.org/10.1128/ecosalplus.ESP-0002-2016.

42. Ribas de Pouplana L, Schimmel P. 2001. Two classes of tRNA synthetases suggested by sterically compatible dockings on tRNA acceptor stem. Cell 104:191–193. https://doi.org/10.1016/S0092-8674(01)00204-5.

43. Bordes P, Cirinesi A-M, Ummels R, Sala A, Sakr S, Bitter W, Genevaux P. 2011. SecB-like chaperone controls a toxin-antitoxin stress-responsive system in Mycobacterium tuberculosis. Proc Natl Acad Sci U S A 108:8438–8443. https://doi.org/10.1073/pnas.1101189108.

44. Volante A, Soberon NE, Ayora S, Alonso JC. 2014. The interplay between different stability systems contributes to faithful segregation: Streptococcus pyogenes pSM19035 as a model. Microbiol Spectr 2(4):PLAS-0007-2013. https://doi.org/10.1128/microbiolspec.PLAS-0007-2013.

45. Hallez R, Geeraerts D, Sterckx Y, Mine N, Loris R, Van Melderen L. 2010. New toxins homologous to ParE belonging to three-component toxin-antitoxin systems in Escherichia coli O157:H7. Mol Microbiol 76:719–732. https://doi.org/10.1111/j.1365-2958.2010.07129.x.

46. Baba T, Ara T, Hasegawa M, Takai Y, Okumura Y, Baba M, Datsenko KA, Tomita M, Wanner BL, Mori H. 2006. Construction of Escherichia coli K-12 in-frame, single-gene knockout mutants: the Keio collection. Mol Syst Biol 2:2006.008. https://doi.org/10.1038/msb4100050.

47. Datsenko KA, Wanner BL. 2000. One-step inactivation of chromosomal genes in Escherichia coli K-12 using PCR products. Proc Natl Acad Sci U S A 97:6640–6645. https://doi.org/10.1073/pnas.120163297.

48. Cherny I, Overgaard M, Borch J, Bram Y, Gerdes K, Gazit E. 2007. Structural and thermodynamic characterization of the Escherichia coli RelBE toxin-antitoxin system: indication for a functional role of differential stability. Biochemistry 46:12152–12163. https://doi.org/10.1021/bi701037e.

49. Semanjski M, Germain E, Bratl K, Kiessling A, Gerdes K, Macek B. 2018. The kinases HipA and HipA7 phosphorylate different substrate pools in Escherichia coli to promote multidrug tolerance. Sci Signal 11:eaat5750. https://doi.org/10.1126/scisignal.aat5750.

50. Cox J, Mann M. 2008. MaxQuant enables high peptide identification rates, individualized p.p.b.-range mass accuracies and proteome-wide protein quantification. Nat Biotechnol 26:1367–1372. https://doi.org/10.1038/nbt.1511.

51. Cox J, Neuhauser N, Michalski A, Scheltema RA, Olsen JV, Mann M. 2011. Andromeda: a peptide search engine integrated into the MaxQuant environment. J Proteome Res 10:1794–1805. https://doi.org/10.1021/pr101065j.

52. Cashel M. 1994. Detection of (p)ppGpp accumulation patterns in Escherichia coli mutants. Methods Mol Genet 3:341–356.

53. Tian C, Roghanian M, Jorgensen MG, Sneppen K, Sorensen MA, Gerdes K, Mitarai N. 2016. Rapid curtailing of the stringent response by toxin-antitoxin module-encoded mRNases. J Bacteriol 198:1918–1926. https://doi.org/10.1128/JB.00062-16.

54. Vizcaíno JA, Csordas A, del-Toro N, Dianes JA, Griss J, Lavidas I, Mayer G, Perez-Riverol Y, Reisinger F, Ternent T, Xu Q-W, Wang R, Hermjakob H. 2016. 2016 update of the PRIDE database and its related tools. Nucleic Acids Res 44:D447–D456. https://doi.org/10.1093/nar/gkv1145.

55. Kitagawa M, Ara T, Arifuzzaman M, Ioka-Nakamichi T, Inamoto E, Toyonaga H, Mori H. 2005. Complete set of ORF clones of Escherichia coli ASKA library (a complete set of E. coli K-12 ORF archive): unique resources for biological research. DNA Res 12:291–299. https://doi.org/10.1093/dnares/dsi012.

56. Gotfredsen M, Gerdes K. 1998. The Escherichia coli relBE genes belong to a new toxin–antitoxin gene family. Mol Microbiol 29:1065–1076. https://doi.org/10.1046/j.1365-2958.1998.00993.x.

57. Lanzer M, Bujard H. 1988. Promoters largely determine the efficiency of repressor action. Proc Natl Acad Sci U S A 85:8973–8977. https://doi.org/10.1073/pnas.85.23.8973.

58. Blattner F, Plunkett GI, Bloch C, Perna N, Burland V, Riley M, Collado-Vides J, Glasner J, Rode C, Mayhew G, Gregor J, Davis N, Kirkpatrick H, Goeden M, Rose D, Mau B, Shao Y. 1997. The complete genome sequence of Escherichia coli K-12. Science 277:1453–1462. https://doi.org/10.1126/science.277.5331.1453.

59. Studier FW, Moffatt BA. 1986. Use of bacteriophage T7 RNA polymerase to direct selective high-level expression of cloned genes. J Mol Biol 189:113–130. https://doi.org/10.1016/0022-2836(86)90385-2.

60. Miroux B, Walker JE. 1996. Over-production of proteins in Escherichia coli: mutant hosts that allow synthesis of some membrane proteins and globular proteins at high levels. J Mol Biol 260:289–298. https://doi.org/10.1006/jmbi.1996.0399.

61. Guzman LM, Belin D, Carson MJ, Beckwith J. 1995. Tight regulation, modulation, and high-level expression by vectors containing the arabinose P(BAD) promoter. J Bacteriol 177:4121–4130. https://doi.org/10.1128/jb.177.14.4121-4130.1995.

62. Bolivar F, Rodriguez RL, Greene PJ, Betlach MC, Heyneker HL, Boyer HW, Crosa JH, Falkow S. 1977. Construction and characterization of new cloning vehicle. II. A multipurpose cloning system. Gene 2:95–113. https://doi.org/10.1016/0378-1119(77)90000-2.